Hardening by ion implantation of VT1-0 alloy having different grain size

Alisa Nikonenko' , Natalya Popova' , Elena Nikonenko' , Mark Kalashnikov' , and Irina Kurzina'

Citation: **1698**, 050003 (2016); doi: 10.1063/1.4937852
View online: http://dx.doi.org/10.1063/1.4937852
View Table of Contents: http://aip.scitation.org/toc/apc/1698/1
Published by the American Institute of Physics

Hardening by Ion Implantation of VT1-0 Alloy Having Different Grain Size

Alisa Nikonenko[1,a)], Natalya Popova[2,3,b)], Elena Nikonenko[2,4,c)], Mark Kalashnikov[3,d)], and Irina Kurzina[1,e)]

[1]*National Research Tomsk State University, 36, Lenin Str., 634050, Tomsk, Russia;*
[2]*Tomsk State University of Architecture and Building, 2, Solyanaya Sq., 634003, Tomsk, Russia;*
[3]*Institute of Strength Physics and Materials Science, SB RAS, 2/4, Akademicheskii Ave., 634021, Tomsk Russia;*
[4]*National Research Tomsk Polytechnic University, 30, Lenin Str., 634050, Tomsk, Russia*

[a)] Corresponding author: aliska-nik@mail.ru;
[b)] natalya-popova-44@mail.ru; [c)] vilatomsk@mail.ru; [d)] kmp1980@mail.ru;[e)] kurzina99@mail.ru

Abstract. The paper presents a transmission electron microscopy (TEM) study of the structural and phase state of commercially pure titanium implanted by aluminum ions. TEM study has been carried out for two types of grains, namely coarse (0.4 μm) and small (0.5 μm). This paper presents details of the yield stress calculations and the analysis of strength components for the both grain types in two areas of the modified layer: at a distance of 0-150 nm (surface area I) and ~300 nm (central area II) from the irradiated surface. It is shown that the ion implantation results in a considerable hardening of the entire thickness of the implanted layer in the both grain types. The grain size has, however, a different effect on the yield stress in areas I and II. Thus, near the ion-alloyed layer, the yield stress decreases with the increase of the grain size, whilst area II demonstrates its increase. Moreover, the contribution to the general hardening of the alloy made by certain hardening mechanisms differs from contributions made by each of these mechanisms in each certain case.

INTRODUCTION

The ion-beam treatment of materials as described in works of [1-5] is currently one of the most intensively developing techniques used for the synthesis of new materials. All experimentally proved models of phase formation at ion implantation are designed basically using coarse-grain metals [2]. However, the decrease of grain sizes, and respectively, the increase of density of grain boundaries and triple points lead to a rapid acceleration of such processes as diffusion, alloying, mixing, formation of secondary phases and defects as observed in works of [1-5], and the emergence of new phases including those not reflected on state diagrams. Thus, a study of phase formation in implanting aluminum ions in titanium materials having various structural conditions (at micro- and meso-levels) is rather relevant. It is possible to assume that physical processes occurred in materials characterized by a heterogeneous condition, i.e. a presence of both small (up to 0.5 μm) and coarse (up to 0.5-5.0 μm) grains or micro- or meso-levels, behave differently as compared to those characterized by a homogeneous condition.

The aim of this study is to analyse and compare the results of research carried out into the microstructure, phase composition, and strength properties of the yield stress, and titanium target in a poly-grained condition before and after the aluminium ion implantation. A poly-grained condition refers to a presence of both small (up to 0.5 μm) and coarse (up to 0.5-5 μm) grains in the material workpiece.

MATERIAL AND METHODS

Workpieces of commercially pure titanium were used in this experiment. These workpieces were obtained by uniaxial isothermal forging combined with reverse rolling as described in the work of Eroshenko *et al*. [6] and the additional annealing at 500°C. Aluminum ions were implanted in titanium workpieces using the new version of the Mevva (Metal Vapor Vacuum Arc) ion source Mevva-V.RU described in detail in the work of Gushenets *et al*. [7]. Titanium workpieces were exposed to ion implantation at temperature 623 K, accelerating

Advanced Materials in Technology and Construction (AMTC-2015)
AIP Conf. Proc. 1698, 050003-1–050003-8; doi: 10.1063/1.4937852

voltage 50 kV, ionic current density 6.5 mA/cm^2, distance 60 cm from the ion-optical system, implantation time 5.25 h, and fluence $1 \cdot 10^{18}$ ion/cm^2. The microstructure and phase composition were studied with the EM-125K transmission electron microscope (TEM) having the accelerating voltage of 120 kV. A study of the microstructure and phase composition of the implanted materials was carried out for two areas of the modified layer, namely: at a distance of 0-150 nm (surface area I) and ~300 nm (central area II) from the irradiated surface.

RESULTS AND DISCUSSION

Conditions described in the work of Kurzina *et al*. [8] for the alloy preparation provide two types of grains retained after the ion implantation. A typical image obtained under TEM and its schematic view are given in Fig. 1 a, b. The size of small grains ranges from 0.1 to 0.5 μm. Their average size is 0.40 μm.

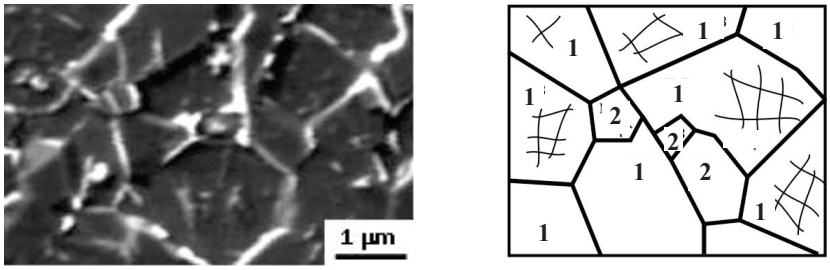

(a) (b)

FIGURE 1. Grained structure after the ion implantation: a - TEM image; b - its schematic view (1 – coarse grains; 2 – small grains)

The size of coarse grains ranges from 0.5 to 5.0 μm. Their average size is 1.40 μm. The content of small grains is not large and comes to 10%. Small grains are mainly located in the boundary triple point intersections of coarse grains. Unimodal functions of the grain-size distribution are presented in Fig. 2 a, b. Maximums of distribution functions are close to their average values.

In this work [8], Kurzina *et al.* observed that the ion implantation lead to a modification of the elementary composition of titanium layers. As is known from the work of Kurzina *et al.* [9], the alloying admixture, namely, aluminum, is distributed non-uniformly both throughout the implanted layers and small and coarse grains of Ti alloy. At first, aluminum forms a solid solution. And the larger the matrix grain the higher the aluminum concentration in the solid solution. Relative to coarse grains, small grains are unified by aluminum. A non-uniform distribution of the alloying admixture along the material results in the different phase composition of small and coarse grains.

Investigations [8] show that at a distance of up to 200 nm from the irradiated surface (area I), both small and coarse grains are not only retained, but the content of small grains even increases by 30% of the total grain content. The average size of both grain types decreases. The both types of grains are also observed in the area II. The content of small grains is the same as before implantation (10%). The average size of coarse grains also remains as before implantation, and the size of small grains is similar to that of the area I.

Functions of the grain-size distribution for areas I and II are presented in Figures 2 c-f. It is clearly seen that these functions are unimodal throughout the implanted layer. Maximums of distribution functions for each grain state in each area are close to their average values.

Aluminum ion implantation in titanium coarse grains results in the formation of secondary phases, namely Ti_3Al, $TiAl_3$ and TiO_2 [8], the total number of which in area I is 3% of the material volume, whilst in area II it is 10%. Ti_3Al-phase is an ordered phase having the superstructure $D0_{19}$ and HCP (hexagonal close-packed) lattice. $TiAl_3$-phase is an ordered phase having the superstructure $D0_{22}$ and body-centered lattice. The electron microscope image of this phase particles is shown in Fig. 3. TiO_2 phase possesses the orthorhombic crystalline lattice. The electron microscope image of this phase particles is shown in Fig. 4 that allows observing two types of TiO_2 particles, i.e. rounded particles located on dislocations and lamellar particles locating inside grains.

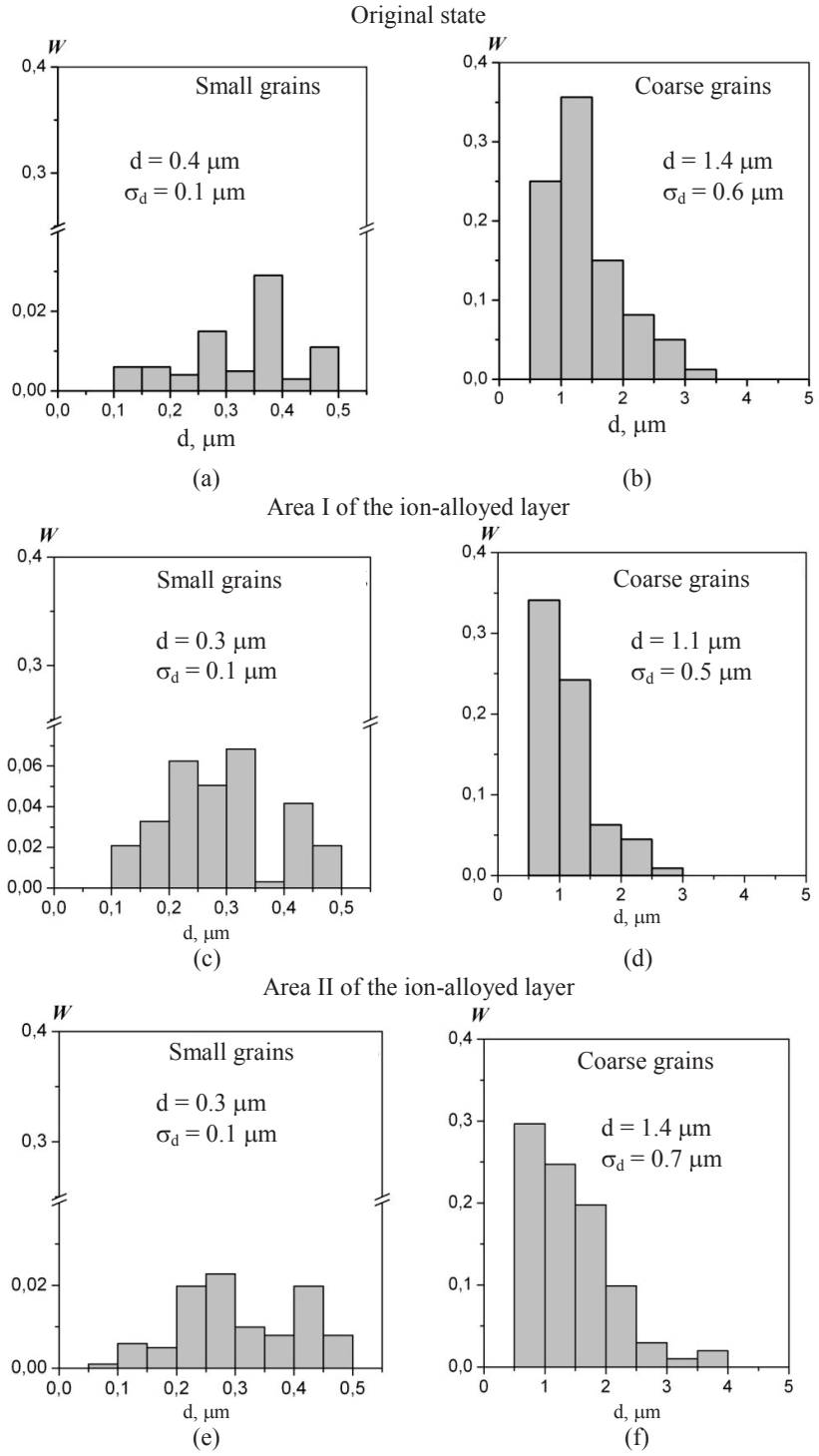

FIGURE 2. Grain-size distribution: a, b – original state; c, d – in ion-alloyed area I; e, f – in ion-alloyed area II

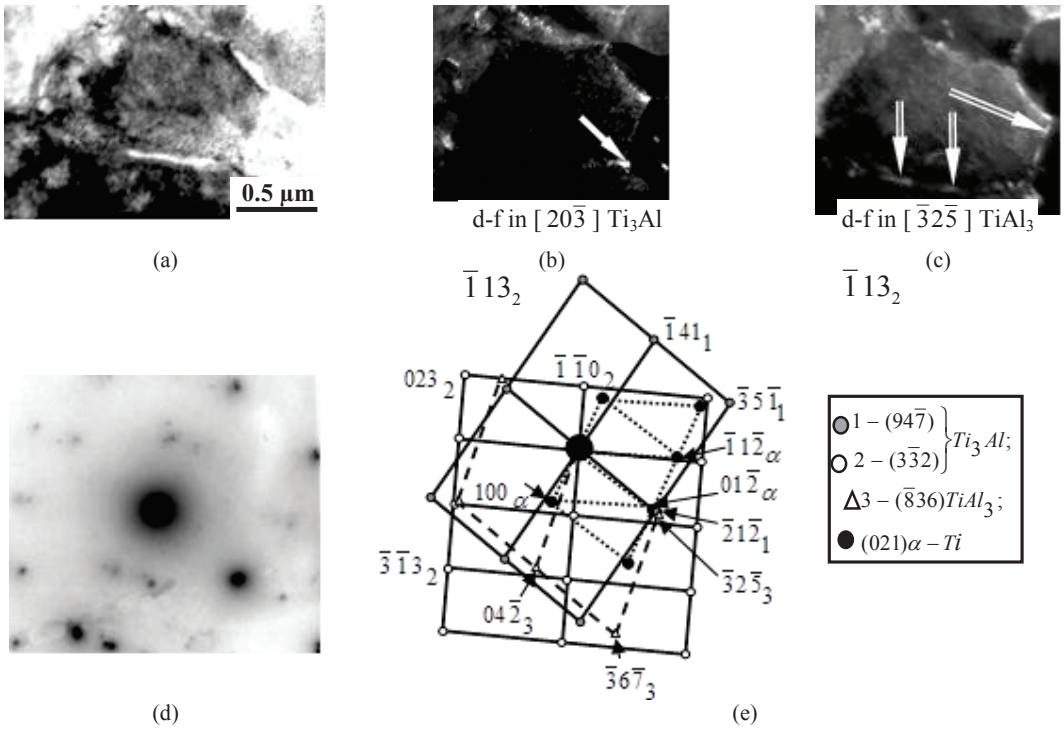

FIGURE 3. Ti_3Al, $TiAl_3$ phase precipitation in α Ti grain. Electron microscope images: a – bright-field image; b, c – dark-field images obtained in Ti_3Al and $TiAl_3$ phase reflections respectively; d, e – micro-diffraction pattern of (a) and its visual display

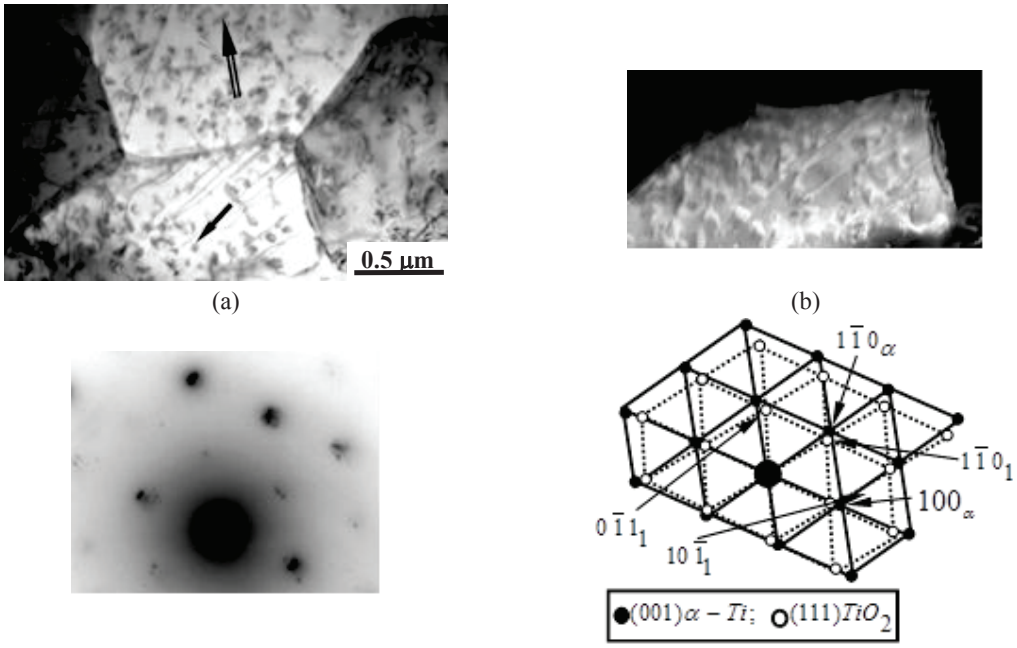

FIGURE 4. TiO_2 phase precipitation in α Ti grain. Electron microscope images: a – bright-field image (single arrow is for rounded and double arrow is for lamellar TiO_2 particles); b – dark-field image obtained in α-Ti and TiO_2 phase reflections; c, d – micro-diffraction pattern and its visual display

Ti_3Al-phase formation is observed throughout the alloyed volume, whilst TiAl3-phase is formed only in the centre of the implanted layer along the grain boundaries. In small grains, these phases are not observed. TiO_2 is formed in all grain types and throughout the alloyed layer.

Thus, small and coarse grains differ not only by their phase composition but also by their amount. It is stated that, first, the larger grain size the larger phase precipitation. Second, in area II of the ion-alloyed Ti layer, the volume fraction of phase precipitation is always higher. Third, TiO_2 particles precipitate most of all in each area of the ion-alloyed Ti layer and in each grain type.

Also, small and coarse grains differ not only by their qualitative and quantitative phase compositions but also by the defect structure. These differences are retained before and after the ion implantation. Dislocations and dislocation entanglements are present in the material before the ion implantation. Dislocation density ρ increases with the decrease of Ti grain size, namely: in coarse grains $\rho = 1.2 \cdot 10^9$ cm^{-2}, while in small grains $\rho = 2.5 \cdot 10^9$ cm^{-2} (Fig. 5 a, curve 1). After the ion implantation, modification of the dislocation structure is observed in the surface layers. Scalar density decreases, while the excessive density increases. The dislocation structure is mostly cross-linked. In area I, the average value of dislocation density ρ is twice as high in small grains as it is in coarse grains (Fig. 5 a, curve 2). Scalar density of dislocations in coarse grains in area II is over four times as high as it is in area I, while in small grains it increases three times (Fig. 1 a, curve 3). Unlike coarse grains, the average value of dislocation density ρ remains higher in small grains. In the whole material this value is three times higher in area II than in area I. Thus, with distance from the irradiated surface, the scalar density of dislocations both in coarse and small grains of α-Ti phase increases with the different intensity, and is higher than that of the original state in both areas (Fig. 5 a).

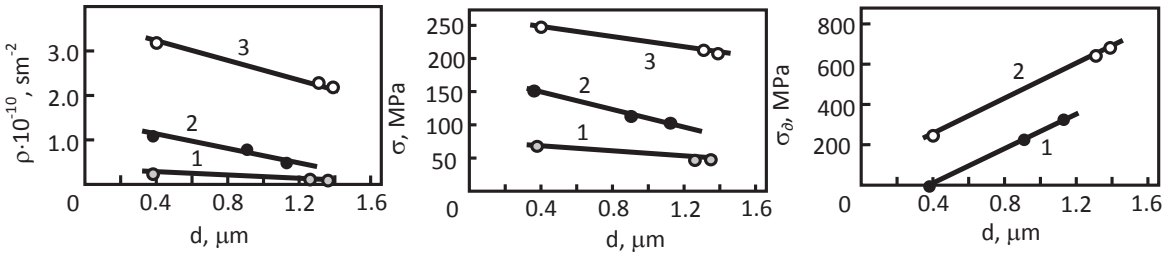

(a) (b) (c)

FIGURE 5. Dependences of scalar density (a), shear stresses (b), and local stresses (c) and the average grain size α-Ti before and after ion implantation: 1 – original Ti specimen; 2 – ion-alloyed layer in area I; 3 – surface layer of the area II

The ion-modified dislocation structure creates internal stresses σ (shear stresses) shown in Figure 5*b*. As this figure shows, first, with distance from the irradiated surface, the value σ increases throughout the material volume. Second, dependences between the value σ and grain sizes are similar to that of the value ρ. After the ion implantation, stresses increase by 3-5 times with distance from the irradiated surface and relative to the original state. Third, small grains are characterized by stresses higher than that of the coarse grains.

The ion-modified dislocation structure together with the scalar dislocation density is characterized by the high excessive density ($\rho_{\pm}$) which enables internal stresses, i.e. couple or local stresses $\sigma_{f.r.}$. The amplitude of couple stresses both in small and coarse grains differs and also at an average, in each area of the implanted alloy. Ion implantation results in the formation of the elastoplastic couple stresses the amplitude of which significantly increases the value of the yield shear stress. At the same time, in coarse grains the elastic component of the couple stress amplitude is over two times higher than the plastic component. In small grains of area I couple stresses are completely absent; while in area II they are present due to dislocation charges (Fig. 5c).

The yield stress can be found from equation (1) based on the obtained quantitative structural parameters for coarse and small grains individually. In this equation, contributions made to hardening by forest dislocations and internal fields are quadratic, all other contributions are additive [10]:

$$\sigma = \Delta\sigma_n + \Delta\sigma_{me} + \Delta\sigma_з + \Delta\sigma_{op} + \sqrt{\left(\Delta\sigma_o^2 + \Delta\sigma_д^2\right)}. \quad (1)$$

where contributions made to hardening by forest dislocations and internal fields are quadratic, all other contributions are additive. This equation covers practically all contributions of resistance to deformation. Here, $\Delta\sigma_{fr}$ is the frictional constraint of dislocations in a crystal lattice of α-Ti phase; $\Delta\sigma_h$ is hardening of the solid solution based on α-Ti atoms of alloying elements (Al, C, O); $\Delta\sigma_f$ is hardening by forest dislocations which cut off slip dislocations; $\Delta\sigma_{f.r.}$ is hardening by far-ranging stress fields; $\Delta\sigma_O$ is hardening by incoherent particles at the dislocation bypass called Orowan mechanism; $\Delta\sigma_g$ is hardening due to grain boundaries.

Calculation results are presented in Figure 6. It should be underlined that this type of alloy is practically a single-phase, namely, α-Ti phase in its original state independently of the average grain size. Hence, the contribution to hardening due to the secondary phases $\Delta\sigma_O$ is not observed. Hardening by far-ranging stress

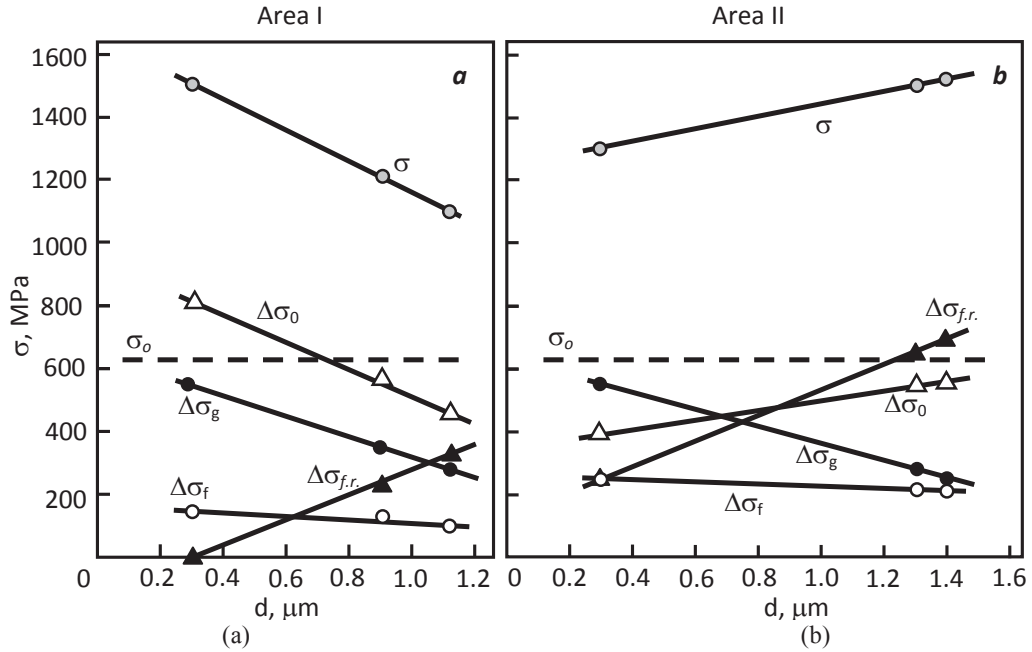

FIGURE 6. Dependence of the yield stress and certain hardening mechanisms contribution upon α-Ti grain size across the ion-alloyed Ti layer: *a* – area I; *b* – are II; σ_o - yield stress of the original alloy

fields is completely absent also. Components $\Delta\sigma_f$ (the frictional constraint of dislocations in a crystal lattice of α-Ti phase) and $\Delta\sigma_h$ (hardening of the solid solution based on α-Ti atoms of alloying elements Al, C, O) also make minimum contribution to hardening, since according to Auger spectroscopy and the XRD analysis [5], carbon and oxygen are not observed in the solid solution of the original alloys. Therefore, hardening of the original material will be defined by $\Delta\sigma_g$ (hardening due to grain boundaries) and $\Delta\sigma_f$ (hardening by forest dislocations, which cut off slip dislocations).

These factors have different behavior for the ion-modified alloy. Since the ion implantation slightly modifies the grain size in the ion-alloyed layer, the grain-boundary strengthening is also modified. Hardening increases due to grain boundaries of α-Ti phase that are the barriers for the flow propagation. It can be described by the Hall-Petch relation [11]:

$$\Delta\sigma_g = k \times d^{-0.5}, \quad (2)$$

where k is the proportionality factor depending on the material purity, the degree of deformation, the type and the structure of grain boundaries, the boundary hardening by the secondary phase particles, and the grain size [9]. It follows from equation (2) that alloy hardening will be stronger in small grains since the density of their boundaries is higher.

According to Koneva *et al.* [10], forest dislocations play the important part in hardening implanted alloys, both for non-polarized (uncharged) and polarized (charged) dislocation ensembles. A non-polarized dislocation ensemble has no excessive dislocations at $\rho_+ = \rho_-$, where ρ_+ and ρ_- are densities of positively and negatively charged dislocations, respectively. The excessive density of dislocations is then $\rho_\pm = \rho_+ - \rho_- = 0$. In this case, the uncharged dislocation ensemble creates a shear stress (for stress fields generated by the structural dislocation) that can be obtained from [12]:

$$\Delta\sigma_f = m\alpha Gb\sqrt{\rho}, \quad (3)$$

where m is the orientation multiplier; α is the dimensionless factor ranged between 0.05-1.0 depending on the type of dislocation ensemble [10]; G is the shear modulus of the material matrix; b is Burgers vector; ρ is the average value of scalar density of dislocations. In case of a charged dislocation ensemble when the excessive density of dislocations equals to:

$$\rho_\pm = \rho_+ - \rho_- \neq 0,$$

long-range couple stresses occur. TEM provides their detection by bend extinction contours observed in the material structure [12,13]. The value of long-range couple stresses can be obtained:

$$\Delta\sigma_{f.r.} = m\alpha_S Gb\sqrt{\rho_{\pm}}, \quad (4)$$

where α_S = 1 is Strunin coefficient [14]. Ion implantation resulted in the accumulation of scalar dislocation density higher than that of the original state of the alloy (Fig. 5*a*). This dislocation structure forms, in turn, higher shear stresses the values of which are also given in Figure 5*b*.

Ion implantation results in polarization of the structural dislocation: bend extinction contours can be observed on TEM images. Thereby, couple (far-ranging) stresses are formed as shown in Figure 5*c*.

Values $\Delta\sigma_f$ and $\Delta\sigma_{f.r.}$ obtained according to (3) and (4) for the different grain sizes as given in Fig. 6, depend on the distance from the irradiated surface.

As stated above, the ion implantation results in the formation of phase compositions. It is detected that the phase composition depends on the average grain size of the alloy. As is known from the work of Honeycomb [15], the dispersion hardening of the alloy depends on the number of particles, their size, distribution, and distance between them, and also the degree of atomic mismatching between the lattices of the precipitate and the matrix. Mechanisms of dispersion hardening are created for incoherent particles when dislocations bypass precipitates and also for coherent particles when dislocations cut off the particles. In alloys under study, TiO_2 particles are incoherent, whilst particles of phases Ti_3Al, and $TiAl_3$ are coherent. Moreover, mechanisms of dispersion hardening are divided into direct (particles are located inside grains) and indirect (particles are located on grain boundaries and triple points). Direct mechanisms lead to the increase of the yield stress of the alloy, while indirect mechanisms affect its strength. In all cases, hardening can be obtained using the Orowan equation [16]:

$$\Delta\sigma_O = 2\lambda Gb/r, \quad (5)$$

where λ = 0.5 is the coefficient accounting for the abovementioned cases; r is the distance between particles.

Calculation results obtained for the contribution of different phases to $\Delta\sigma_O$ value after the implantation of aluminum ions in VT1-0 alloy are presented in Fig. 6.

CONCLUSION

Results of calculations showed that the ion implantation both in coarse and small grains lead to the significant hardening of the alloy over the whole thickness of the implanted layer. The grain size has, however, a different effect on the yield stress in areas I and II. Thus, near the ion-alloyed layer, the yield stress decreases with the increase of the grain size, whilst area II demonstrates its increase. It was shown that before as well as after the ion implantation, the increase of the grain size provided the decrease of the alloy hardening. Moreover, the contribution to the general hardening of the alloy made by certain hardening mechanisms is different, and contributions made by each of these mechanisms in each certain case differs also.

ACKNOWLEDGEMENT

This work was carried out within the governmental contract No. 3.295.2014/K of the Ministry of Education and Science of the Russian Federation.

REFERENCES

1. I. Tsiganov, E. Wieser, W. Matz, A. Mücklich, H. Reuther, M.T. Pham and E. Richter, Thin Solid Films **376, 1-2,** 188-197 (2000).
2. V.A. Gribkov, F.I. Grigor′ev, B.A. Kalin and V.L. Jakushkin, *Perspektivnie radiacionno_puchkovie tehnologii obrabotki materialov* (Kruglyy god, Moscow, 2001), 528 p.
3. F.F. Komarov, *Fizicheskie processi pri ionnoi implantacii v tverdie tela* (Tekhnoprint, Minsk, 2001), 392p.
4. I.A. Kurzina, Yu.P. Sharkeev and E.V. Kozlov, "*Formirovanie nanointermetallidnih faz v usloviyah ionnoi implantacii*" in *Struktura i svoystva perspektivnykh materialov* / Eds. A.I. Potekaev (YTL, Tomsk, 2007), pp.159-195.
5. I.A. Kurzina, N.A. Popova, M.P. Kalashnikov, K.P. Savkin, I.A. Bozhko, E.L. Nikonenko, G.Yu. Yushkov, E.M. Oks, E.V. Kozlov and Yu.P. Sharkeev, Izv. Vuzov. Fizika **11/3,** 112-119 (2011).
6. A.Yu. Eroshenko, Yu.P. Sharkeev, A.I. Tolmachev, G.P. Korobitsyn and V.I. Danilov, Advanced Materials **7**, 107-112 (2009).
7. V.I. Gushenets, A.G. Nikolaev, E.M. Oks, L.G. Vintizenko, G.Yu. Yushkov, A. Ozterhan and I.G. Brown., Rev. Sci. Instrum **77**, 6. 063301 (1-3) (2006).
8. I.A. Kurzina, E.V. Kozlov, N.A. Popova, M.P. Kalashnikov, E.L. Nikonenko, K.P. Savkin, E.M. Oks and Yu.P. Sharkeev, Bulletin of the Russian Academy of Sciences: Physics **76**, 11. 1238-1245 (2012).

9. I.A. Kurzina, E.V. Kozlov, Yu.P. Sharkeev, S.V. Fortuna, N.A. Koneva, I.A. Bozhko and M.P. Kalashnikov, *Nanokristallicheskie intermetallidnie i nitridnie strukturi_ formiruyuschiesya pri ionno_plazmennom vozdeistvii* (Publ YTL, Tomsk, 2008), 324 p.
10. N.A. Koneva and E.V. Kozlov, "*Dislokacionnaya struktura i fizicheskie mehanizmi uprochneniya metallicheskih materialov*" in *Advanced Materials* (manual) / Eds. D.L. Merson (Publisher TSU, MISA, Tula, 2006), pp. 267-320.
11. D. Mac Lin, *Mechanical properties of metals* (Metallurgy, Moskow, 1965), 431 p.
12. N.A. Koneva and E.V. Kozlov, Izv. Vuzov. Fizika **3,** 56-70 (1991).
13. N.A. Koneva and E.V. Kozlov, Izv. Vuzov. Fizika **3** (application), 52-71 (2002).
14. B.N. Strunin, FTT **9**, 3, 805-812 (1967).
15. R.W.K. Honeycombe, The plastic deformation of metals (Wiley, Moskow, 1972), 408 p.
16. M.I. Goldstein and V.M. Farber, *Dispersionnoe uprochnenie stali* (Metallurgy, Moscow, 1979), 208 p.